Olfactory cortical neurons read out a relative time code in the olfactory bulb

Rafi Haddad[1], Anne Lanjuin[1], Linda Madisen[2], Hongkui Zeng[2], Venkatesh N Murthy[1] & Naoshige Uchida[1]

Odor stimulation evokes complex spatiotemporal activity in the olfactory bulb, suggesting that both the identity of activated neurons and the timing of their activity convey information about odors. However, whether and how downstream neurons decipher these temporal patterns remains unknown. We addressed this question by measuring the spiking activity of downstream neurons while optogenetically stimulating two foci in the olfactory bulb with varying relative timing in mice. We found that the overall spike rates of piriform cortex neurons (PCNs) were sensitive to the relative timing of activation. Posterior PCNs showed higher sensitivity to relative input times than neurons in the anterior piriform cortex. In contrast, olfactory bulb neurons rarely showed such sensitivity. Thus, the brain can transform a relative time code in the periphery into a firing rate–based representation in central brain areas, providing evidence for the relevance of a relative time–based code in the olfactory bulb.

A fundamental question in neurobiology is how external stimuli are coded by the activity of neurons in the brain. It has been thought that firing rates over a relatively long time window (several hundreds of milliseconds) code the information about incoming sensory inputs (rate coding)[1]. However, it has also been recognized that sensory stimuli elicit distinct temporal patterns of spikes that are not directly related to stimulus dynamics[2,3]. These observations have led to the idea that the exact timing of spikes or their relative timing across neurons can form a neural code for non-temporal features of stimuli (temporal coding). Temporal coding has various computational advantages over a simpler firing rate–based code, including higher rates of information transmission[4] and invariance to irrelevant stimulus features[5].

In the olfactory bulb, odor stimulation evokes odor-specific temporal patterns of activity at both the levels of the olfactory nerve inputs (activation of glomeruli)[6,7] and the outputs (spiking of mitral and tufted cells)[2,6,8–10]. These temporal modulations occur in the time frame of a single sniff cycle (~200 ms during rapid sniffing) and a substantial amount of information can be extracted from such temporal patterns at the resolution of tens of milliseconds[11,12]. Thus, odor information can, in principle, be coded by temporal patterns of activity in the olfactory bulb. However, the functional relevance of specific temporal codes remains to be established. For a temporal code to be useful, its receiver must be able to decipher it[13,14]. A recent study has shown that, in the piriform cortex, the canonical olfactory cortex, firing rates over the entire sniff cycle, but not the timing of spikes, convey the bulk of odor information[15]. In addition, previous studies using odor mixtures[16,17], electrical stimulations in slice preparations[18,19] and glutamate uncaging in the olfactory bulb *in vivo*[20] have examined how PCNs integrate multiple inputs from the olfactory bulb. These studies have shown that simultaneous activations of specific inputs cause both supralinear and sublinear responses in the

piriform cortex. However, whether the relative timing of glomerular activations, particularly the order of glomerular activations, is important for information transmission remains unknown. We tested the hypothesis that relative timing of glomerular activations in the olfactory bulb is transformed into different firing rate responses in the piriform cortex.

We optogenetically stimulated the olfactory bulb with spatio-temporally dynamic patterns of light[13,21] and examined whether the downstream neurons respond differently depending on the relative timing of activations in the olfactory bulb. We found that many neurons in the piriform cortex responded with different firing rates depending on the order and the lag of stimulations in the olfactory bulb. In contrast, olfactory bulb neurons (OBNs) rarely showed such sensitivity. These results indicate that relative spike time information in the olfactory bulb constitutes an important part of an odor code.

RESULTS

Optogenetic stimulation of olfactory bulb

We optogenetically activated the olfactory bulb in transgenic mice expressing channelrhodopsin-2 (ChR2), a light-gated ion channel, in olfactory receptor neurons (ORNs; **Fig. 1a**,**b**)[21]. Spatial and temporal control of stimulation was achieved by projecting temporally varying two-dimensional light patterns onto the dorsal surface of the olfactory bulb using digital micromirror technology[13,21]. Spiking activity was recorded extracellularly from mitral and tufted cells in the olfactory bulb or neurons in the anterior and posterior subdivisions of the piriform cortex (aPC and pPC; **Supplementary Fig. 1**). Optical stimulation with a single square spot (150 μm, duration of 100 ms) triggered responses both in mitral and tufted and piriform cortex cells. Mitral and tufted cells were typically activated by only a few confined spots that were close to the recording electrode, whereas piriform cortex cells were sometimes excited by several spatially segregated locations

---

[1]Center for Brain Science, Department of Molecular and Cellular Biology, Harvard University, Cambridge, Massachusetts, USA. [2]Allen Institute for Brain Science, Seattle, Washington, USA. Correspondence should be addressed to N.U. (uchida@mcb.harvard.edu).

Figure 1 Characterization of responses to single spot optogenetic activation of olfactory nerve input. (**a**) Experimental setup. Light (cyan) was focused on the surface of the olfactory bulb. Mice expressing ChR2 in ORNs (*Omp-ChR2*) were used. Spiking activity was recorded extracellularly from mitral and tufted (M/T) cells in the olfactory bulb (1) and neurons in the aPC (2) and pPC (3). OB, olfactory bulb; OE, olfactory epithelium; PD, photodiode. (**b**) Fluorescence image of the olfactory bulb in an *Omp-ChR2* mouse. Yellow indicates the location of ChR2 tagged with a yellow fluorescent protein (ChR2-YFP). ChR2 was located exclusively in the glomerular layer (GL). EPL, external plexiform layer; GRL, granule cell layer; MCL, mitral cell layer. Scale bar represents 100 μm. Sections from $n > 20$ mice were examined. (**c**) Left, two-dimensional light activation map for an example neuron in olfactory bulb. Each pixel represents the average firing rate change relative to baseline caused by activation of each olfactory bulb spot. The values were obtained using a 100-ms window after light onset, averaged over 20 randomly interleaved repetitions. The yellow and cyan represent an increase and decrease from baseline, respectively. The range of the color scale corresponds to ±5 s.d. of the baseline activity. The total area scanned for an experiment was determined by the size of the craniotomy. Middle and right, peri-event time histograms (PETHs, mean ± s.e.m.) and raster plots of excitatory and inhibitory spots. Each tick mark represents one spike. The timing of light stimulation is indicated by the cyan bar. The locations of the spots are indicated on the light activation map on the left. This neuron was excited by two spots and inhibited by one spot (*$P < 0.05$, $t_{19} > 2.1$, t test, corrected for multiple comparisons using Bonferroni correction, $n = 20$ repetitions). (**d**) Results from an example PCN. An olfactory bulb was optically stimulated while the activity of a PCN was recorded. This neuron was excited by six spots (*$P < 0.05$, $t_{14} > 2.3$, t test, Bonferroni correction, $n = 15$ repetitions). None of the spots caused a significant inhibitory response in this neuron ($P > 0.05$, t test). PC, piriform cortex. (**e**) Percentage of excitatory spots in single-spot scanning experiments (*$P < 0.05$, t test, $n = 15–20$ repetitions, $n = 29$ OBNs, $n = 25$ aPC neurons, $n = 22$ pPC neurons). The central mark indicates the median and the edges of the box are 25th and 75th percentiles. Each experiment contained 42–60 total spots. Excitatory spots were more prevalent in aPC and pPC than in olfactory bulb (olfactory bulb versus aPC, $Z = 3.75$, $P = 0.00017$; olfactory bulb versus pPC, $Z = 2.1$, $P = 0.031$; Mann-Whitney U test). Dotted lines inside the bars represent the FDRs. The vertical line indicates the maximum and minimum values of non-outliers. Points were considered to be outliers if they were larger than $b + 1.5(b − a)$ or smaller than $a − 1.5(b − a)$, where a and b are the 25th and 75th percentiles, respectively. *$P < 0.05$, ***$P < 0.001$. (**f**) Percentage of inhibitory spots in single-spot scanning experiments. Data are presented as in **e**. Inhibitory spots were more prevalent in olfactory bulb than piriform cortex (olfactory bulb versus aPC, $Z = −4.6$, $P = 3.6 \times 10^{-6}$; olfactory bulb versus pPC, $Z = −4.2$, $P = 1.8 \times 10^{-5}$; Mann-Whitney U test).
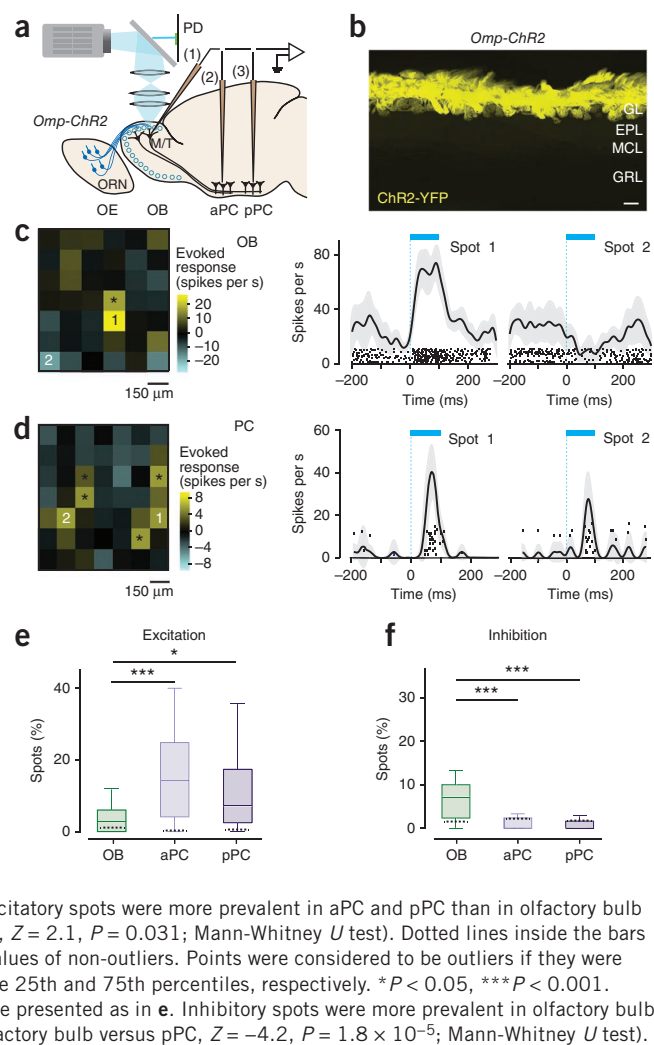
in the olfactory bulb (**Fig. 1c,d**). The fraction of excitatory spots was larger in PCNs than in OBNs (**Fig. 1e**). We also found that activation of some spots suppressed the spontaneous firing of recorded neurons ($P < 0.05$, t test, $n = 20$ repetitions; **Fig. 1d**). Such inhibition was more evident in OBNs than in PCNs (**Fig. 1f**). Previous studies[20,22] observed less frequent excitation or inhibition in the piriform cortex and inhibition in olfactory bulb in response to a single spot activation of the olfactory bulb. This difference may be a result of a slightly larger spot size or a larger number of repetitions used in our study.

To test whether neurons are sensitive to relative timing of olfactory nerve input activation, we optically stimulated two spots of the olfactory bulb with varying relative onset timings (for example, $\Delta t = 0, \pm16.6, \pm33.3, \pm50, \pm66.6$ and ±83 ms; **Fig. 2a–e**). The range of Δt was chosen on the basis of previous studies that have shown that onset latencies of glomerular activation vary on a 50–150-ms time-scale[6,7,23]. To mimic the timescale of olfactory nerve input activations by odors, we illuminated each spot for a relatively long duration on the timescale of a sniff[24,25] (83.3 ms). This design ensured that experimental conditions varied only in terms of relative timing and that the total amount of light was equal in all conditions. To increase the chance of observing any activation, we tested three pairs of spots for each neuron. For comparison, we also examined the response to each spot alone. Single spot stimulation caused mitral and tufted cell activations lasting 60 ± 11 ms (the half maximum width, mean ± s.d.), comparable

to odor responses during natural sniffing[12]. The magnitude of evoked response was moderate and comparable to those observed during odor stimulations[12,26,27] (**Supplementary Fig. 2**). The latency of excitatory responses was short and had small jitter (10 ± 5.8 ms, mean ± s.d.). The time to reach the half maximum firing rate was 21.9 ± 5.7 ms. Inhibitory responses were slightly slower and had slightly more jitter (30 ± 20.8 ms), likely because the ability to detect inhibitory responses is largely limited by spontaneous firing rates.

We constructed a temporal tuning curve (TTC) for each spot pair (76, 114 and 129 TTCs from 45, 47 and 63 neurons in olfactory bulb, aPC and pPC, respectively; **Fig. 2f–i**). TTCs were obtained by counting the number of spikes in a window that covers the period of optical stimulation response (duration = 200 ms). This approximates the timescale relevant for simple perceptual decisions[7,25]. This analysis discards fine temporal patterns and tests whether information regarding relative timing of activations becomes available in the form of firing rates.

PCNs responses depend on the order of input activations

We observed that OBNs' TTCs tended to be flat (**Fig. 2f**), whereas PCNs' TTCs revealed much more shape variability in and across neurons (**Fig. 2g–i** and **Supplementary Fig. 3**). To quantify this, we obtained the slopes of the lines fitted to the positive and negative Δt, separately. This analysis confirmed that OBNs' TTCs tended to be flat (**Fig. 3a–c**), indicating that their responses do not depend on the lag

Figure 2 Acquisition of TTCs for olfactory bulb and PCNs. (**a**) Experimental design for testing temporal sensitivity. Each spot was illuminated for 83.3 ms (five projector frames at 60 Hz). Two spots in the olfactory bulb were illuminated with varying orders and lags. Lags used for the main experiment were 17, 33, 50 and 67 ms. In some experiments, larger lags were also included. For each lag, we tested the response to activation of spot A followed by B (A→B, positive Δt) and the reversed order (B→A, negative Δt). We also tested the response to each spot alone (A or B) and to simultaneous activation of the two spots (A and B, $\Delta t = 0$). (**b**–**e**) Example raster plots of one olfactory bulb (OB, **b**), one aPC (**c**) and two pPC neurons (**d**,**e**). Cyan and magenta bars indicate the timing of light stimulation of spots A and B, respectively. Each dot represents a spike and each row represents one trial. Black lines separate between the different lags. The Δt values are indicated on the right. The experiments shown in **b** and **c** did not include $\Delta t = \pm 83$ ms. (**f**–**i**) TTCs of the neurons shown in **b**–**e**. The total spike counts in the 200-ms analysis window were used to calculate the firing rate. The baseline firing rates in the 200-ms time window before optical stimulation were subtracted. Magenta, spot A alone; cyan, spot B alone; blue, positive Δt (A→B); red, negative Δt (B→A); black, simultaneous stimulation of A and B ($\Delta t = 0$). Data are presented as mean ± s.e.m. ($n = 40$ repetitions). The dashed horizontal lines represent the sum of the responses to spot A alone and B alone (that is, r(A) + r(B)).
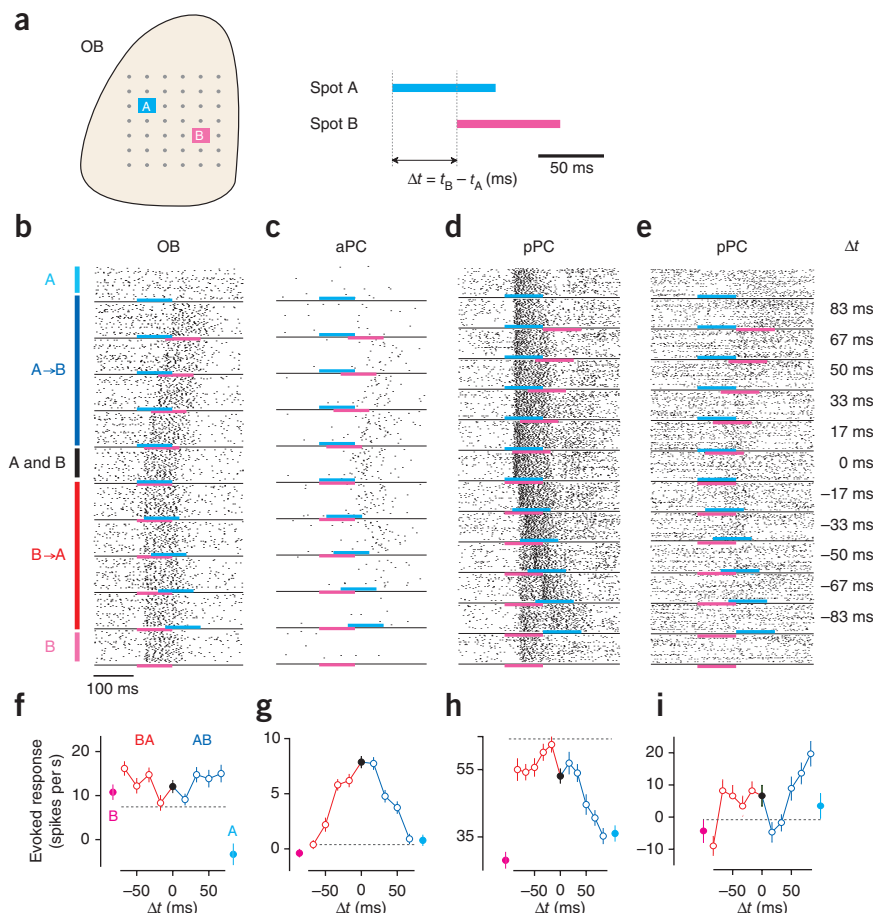
and order of glomerular activation. In contrast, many PCNs showed negative slopes in TTCs (45% of all spot pairs, and 42% of spot pairs in which both spots were responsive, $P < 0.05$, regression analysis, responsive spot was determined by t test, $P < 0.05$, $n = 40$ repetitions per TTC, from 76 total TTCs). Furthermore, a relatively large fraction of spot pairs showed supralinear interactions at zero lag (~30% of all spot pairs, and 26% of spot pairs in which both spots were responsive, t test, $P < 0.05$, $n = 40$ repetitions; aPC, $n = 114$ spot pairs; pPC, 129 spot pairs; **Fig. 3d**–**f** and **Supplementary Fig. 4a,b**)[19,20]. Similar conclusions were obtained when we used analyses that did not depend on binary categorization using a particular P value or on linear fitting (**Supplementary Fig. 4c**–**f**).

Notably, we also found that the TTCs of many PCNs were asymmetric around $\Delta t = 0$. That is, many PCNs showed different responses depending on the order of the two-spot activations (**Figs. 2h,i** and **4a**–**e**). To identify asymmetric TTCs, we devised two complementary tests that captured different aspects of asymmetry (**Supplementary Fig. 5**). First, we tested whether any of the positive Δt values elicited a significantly different response compared with the corresponding negative Δt (t test, Bonferroni correction for the number of Δt). This test looks for an order-sensitive response that is specific to a given lag(s), or lag-specific asymmetry (**Figs. 2h,i** and **4a,d,e**).

Second, in some cases, the overall shape of the positive and negative TTCs were different, although responses at none of the lags crossed our stringent statistical threshold (**Fig. 4b,c**). To capture these cases, we tested whether the fitted lines for positive and negative Δt differed significantly in their slopes and/or intercepts using the analysis of covariance (ANCOVA, $P_A < 0.05$, global asymmetry). The test for global asymmetry

was significant in the first experiment, but not in the second, solely as a result of the different lags used in the second experiment (**Fig. 4e**).

Sensitivity to relative timing is maximal in pPC neurons

Applying the above two criteria, we found that a significant fraction of spot pairs in the piriform cortex had asymmetric TTCs (aPC, 23.3% of TTCs; pPC, 32.3%; $P < 0.0001$ for spot pairs in aPC and pPC compared with 8% expected false discovery rate (FDR)[28] using trial shuffled data, binomial test; **Fig. 4f**). Similar results were obtained in terms of the fraction of neurons that had at least one asymmetric TTC (**Fig. 4f**). These fractions were surprisingly high considering that the majority of olfactory bulb spot stimulation did not elicit any responses in PCNs (**Fig. 1e,f**), presumably as a result of relatively sparse or weak connectivity between olfactory bulb and piriform cortex. Thus, the probability that a randomly chosen spot pair interacts is expected to be low. Indeed, when we analyzed spot pairs that elicited either an excitatory or an inhibitory response in the recorded PCN, the probability of obtaining asymmetric TTCs increased (28% in aPC and 40% in pPC, compared to 5% in olfactory bulb; **Supplementary Fig. 6a**). Overall, the two criteria for detecting asymmetric TTCs captured largely overlapping populations (~70%; **Supplementary Fig. 6b,c**). Notably, the fraction of spot pairs with asymmetric TTCs was significantly higher in pPC than in aPC ($P = 0.023$, binomial test) and did not depend on the distance between the spots (**Fig. 4f,g**). In a stark contrast, very few spot pairs in olfactory bulb showed order sensitivity (11.3%, $P = 0.00072$ compared to aPC, binomial test; **Fig. 4f**). These findings can be replicated using independent methods that do not involve linear fitting or the two specific criteria used for detecting order selectivity (**Supplementary Fig. 6d**).
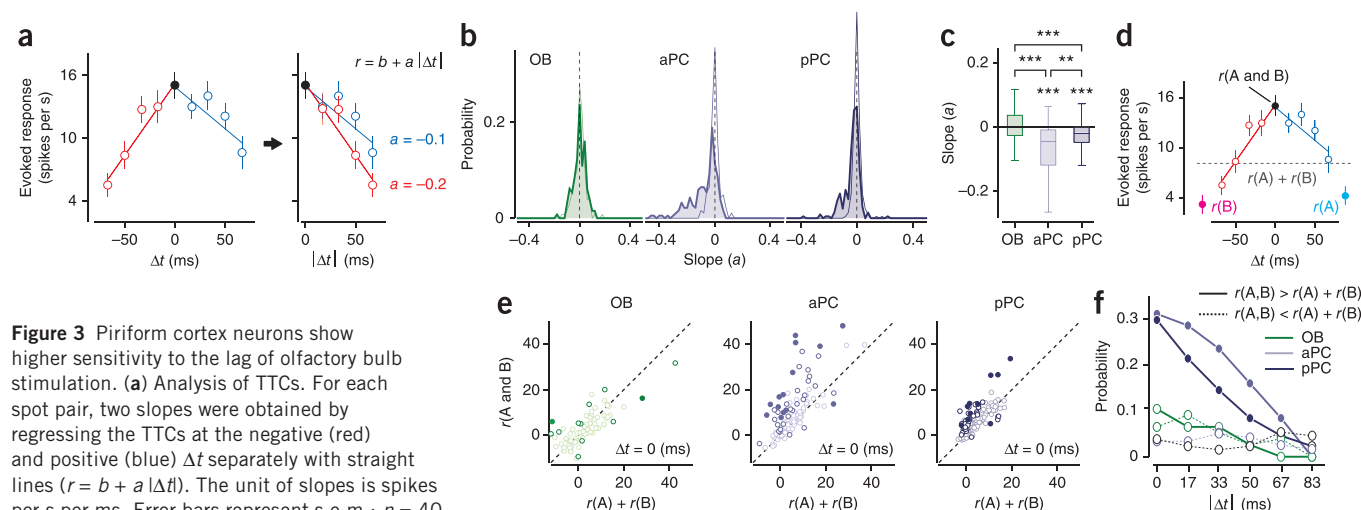
Figure 3 Piriform cortex neurons show higher sensitivity to the lag of olfactory bulb stimulation. (**a**) Analysis of TTCs. For each spot pair, two slopes were obtained by regressing the TTCs at the negative (red) and positive (blue) Δt separately with straight lines ($r = b + a|\Delta t|$). The unit of slopes is spikes per s per ms. Error bars represent s.e.m.; $n = 40$ repetitions. (**b**) Distributions of slopes of TTCs for olfactory bulb, aPC and pPC neurons. Thin lines indicate the distribution of the slopes with the data shuffled with respect to Δt. The distribution of the slopes of the fitted lines was mostly near zero for OBNs (−0.0005 ± 0.5, t test against zero, $t_{151} = 0.14$, $P = 0.89$, $n = 152$ fitted lines), whereas aPC and pPC neurons' slopes were significantly shifted below zero (aPC, −0.069 ± 0.09, t test against zero, $t_{227} = 11.07$, $P = 4.6 \times 10^{-23}$, $n = 228$ fitted lines; pPC, −0.042 ± 0.06, $t_{257} = 9.8$, $P = 1.0 \times 10^{-19}$, $n = 258$ fitted lines). The distribution of the slopes of OBNs was similar to those obtained in the surrogate data, suggesting that the variability in slopes originates mostly from the finite number of trials in the data. In contrast, the distribution of the slopes for PCNs was shifted compared with trial-shuffled surrogate data, and the mean slopes were significantly smaller than those of the surrogate data ($P < 0.001$, Kolmogorov-Smirnov test for both aPC and pPC, $n = 228$ and 258 fitted lines for pPC and pPC, respectively), whereas that of olfactory bulb was not ($P = 0.63$, Kolmogorov-Smirnov test, $n = 152$ fitted lines). (**c**) Box plots of the slopes of TTCs in the three brain regions. The mean slopes of aPC and pPC neurons were significantly negative ($P < 0.001$ for both aPC and pPC, t test against zero). The average slopes of OBNs were significantly different from those of aPC and pPC neurons ($Z > 6.2$, $P < 3.5 \times 10^{-10}$, for both olfactory bulb versus aPC and olfactory bulb versus pPC, Mann-Whitney U test), whereas aPC slopes were also significantly different from pPC slopes ($Z = −2.82$, $P = 0.0047$, aPC versus pPC, Mann-Whitney U test). Data presented as in **Figure 1e**. **$P < 0.01$, ***$P < 0.001$. (**d**) An example TTC to illustrate the analysis. r(A), response to A; r(B), response to B; r(A and B), response to simultaneous activation of A and B ($\Delta t = 0$). The gray dashed line indicates the arithmetic sum of the response to spot A and B (r(A) + r(B)). (**e**) Comparison between the sum of the responses to spots A and B (r(A) + r(B)) and the actual response for simultaneous presentation of spots A and B (r(A and B), $\Delta t = 0$. Each circle represents a spot pair. Open and filled dark circles indicate supralinear facilitation or suppression ($P < 0.05$, t test, not corrected (open) or corrected (filled) for multiple comparisons, $n = 40$ repetitions). In aPC and pPC neurons, the response to r(A and B) tended to be larger than that to r(A) + r(B). (**f**) Percentage of spot pairs in which the responses to two-spot stimulations (r(A, B)) were greater than r(A) + r(B) (that is, supralinear, t test, $P < 0.05$, $n = 40$ repetitions, solid lines) or smaller (sublinear, t test, $P < 0.05$, $n = 40$ repetitions, dashed lines) for a given lag (Δt). The average trial-shuffled control values in all three brain areas resulted in ~3% (range: 1–8%).

We also found that some TTCs peaked at a nonzero lag (**Fig. 4d,e**). We identified this type of asymmetry using the criterion that the response at a nonzero Δt was significantly higher than that at $\Delta t = 0$ (one sided t test between each Δt versus $\Delta t = 0$, Bonferroni correction for the number of Δt and spot pairs). A significant fraction of neurons peaked at a nonzero Δt (aPC, ~18%; pPC, ~11%; compared with ~4% FDR using trial-shuffled data, $P < 0.0021$ for spot pairs and neurons in aPC and pPC, binomial test; **Fig. 4h**).

The apparent lack of interactions (low order sensitivity) in the olfactory bulb was somewhat surprising to us given that inhibition was observed more frequently in the olfactory bulb than in piriform cortex (**Fig. 1f**). It is unlikely that this result is an artifact of unnatural stimulus (for example, over-excitation of mitral and tufted cells that overwhelms lateral inhibition), as the magnitude of the responses in mitral and tufted cells was modest and comparable to those during odor stimulations[12,26,27]. To directly address this issue, we performed a control experiment in which light intensity was reduced for the excitatory spot while remaining high for the inhibitory spot for the same mitral and tufted cell (**Supplementary Fig. 7a**). First, excitatory-inhibitory spot pairs in the original light condition yielded only 11% of order-sensitive cases. Although reducing the light intensity for an excitatory spot decreased the magnitude of light-evoked responses (**Supplementary Fig. 2j,k**), the frequency of order-sensitive cases remained very low (8.8%, $n = 34$ spot pairs). We then simultaneously stimulated multiple inhibitory spots to

increase the inhibitory inputs (**Supplementary Fig. 7b–d**), which yielded similar results (9.3% order sensitive, $n = 21$ spot pairs; FDR, 8.3%). These results indicate that inhibitory circuits in the bulb are not important for the generation of strong order sensitivity. We note that the lack of strong temporal interaction in the olfactory bulb might be a result of a possible effect of anesthesia on inhibition. However, under the same conditions, PCNs showed much higher order and lag sensitivity.

These results indicate that the responses of many PCNs are sensitive to the order and the lag of glomerular activation, whereas the responses of OBNs are largely insensitive to the order and the lag of glomerular activation. Furthermore, pPC neurons were more order sensitive than aPC neurons.

The role of inhibition in generating order sensitivity
What are the mechanisms that generate asymmetric TTCs? Given that previous studies have shown that the responsiveness of PCNs is shaped by inhibition[18,29–32], we next examined asymmetric TTCs in more detail for evidence of inhibitory interactions (**Fig. 5**). In some cases, each of the two spots excited a neuron, and the overall magnitudes of the responses were similar for shorter lags ($|\Delta t| \leq 50$ ms) regardless of the order (**Fig. 5a**). However, the response became asymmetric with larger lags (lags 67 ms or larger; **Fig. 5a**). Such a difference can be a result of the lack of response to the second stimulus in one order, but not the other (**Fig. 5a**). This asymmetric responsiveness could

Figure 4 Order–specific responses of PCNs. (**a**) TTC of an aPC neuron. Data are presented as in **Figure 2**. The responses to B→A stimulation (red) remained flat for all lags, whereas the responses to A→B (blue) decreased as the lag increased. This asymmetry was captured by both the global and lag-specific tests ($P_A = 0.00013$, $F_{1,446} = 14.8$, ANCOVA; $\Delta t = \pm67$, $P = 0.0023$, $t_{88} = 3.1$; $\Delta t = \pm83$ ms, $P = 0.00040$, $t_{88} = 3.7$; t test, $n = 45$ repetitions for both). P_A indicates the P value in ANCOVA. The P values for lag-specific comparisons are shown only when they are smaller than the criterion (t test, corrected for the number of $|\Delta t|$ values, Bonferroni correction). Data are presented as mean ± s.e.m. (**b**) TTC of a pPC neuron. The responses to B→A were similar to $r(A) + r(B)$ (the gray dashed line), whereas the responses for the opposite order (A→B) decreased as the lag increased ($F_{1,316} = 5.4$, $P_A = 0.019$, ANCOVA, $n = 40$ repetitions). (**c**) TTC of a pPC neuron. The responses to B→A were generally weaker than those to A→B. This asymmetry was captured by the global tests ($P_A = 0.041$, $F_{1,316} = 4.2$, ANCOVA). The lag-specific differences at $\Delta t = \pm67$ and ±50 ms ($\Delta t = \pm67$, $P = 0.023$, $t_{78} = 2.3$; $\Delta t = \pm50$, $P = 0.025$, $t_{78} = 2.3$; t test, $n = 40$ repetitions) did not cross the criterion ($P < 0.0125$, Bonferroni corrected; **Supplementary Fig. 5**). (**d**) TTC of a pPC neuron. This neuron responded maximally when spot B was stimulated 67 ms after spot A ($P = 0.0055$, $t_{78} = 2.8$, t test between $\Delta t = 67$ ms and $\Delta t = 0$ ms, $n = 40$ repetitions) and did not respond to activation of either of the spots or to simultaneous stimulation of both spots. This asymmetry was captured by the lag-specific test ($\Delta t = \pm50$, $P = 0.00042$, $t_{78} = 3.6$; $\Delta t = \pm67$ ms, $P = 0.0062$, $t_{78} = 2.8$; t test, $n = 40$ repetitions for both). The global test was not significant ($P_A = 0.062$, $F_{1,316} = 3.5$, ANCOVA). (**e**) Left, TTC of a pPC neuron. This neuron responded strongly only when A started 50–83 ms after spot B ($\Delta t = \pm50$, $P = 0.038$, $t_{78} = 2.1$; $\Delta t = \pm66$, $P = 0.00034$, $t_{78} = 3.7$; $\Delta t = \pm83$, $P = 0.0062$, $t_{78} = 2.8$; t test, $n = 40$ repetitions for all). The responses peaked at 67 ms ($P = 0.00099$, $t_{78} = 3.4$, t test between $\Delta t = 67$ ms and $\Delta t = 0$ ms, $n = 40$ repetitions). Right,

TTC of the shown at left, but tested with a different set of lags in an independent experiment. The peak at $\Delta t = 67$ ms was reproduced ($P = 0.0027$, $t_{78} = 3.1$, t test between $\Delta t = -67$ ms and $\Delta t = 0$ ms, $n = 40$ repetitions), response decreased with longer Δt. (**f**) Percentage of order-sensitive cases calculated in terms of spot pairs (white bars) and neurons (gray bars) in each brain area (Bonferroni corrected t test for all $\pm\Delta t$ and $P_A < 0.05$, ANCOVA, $n = 76$, 114, 129 spot pairs and $n = 45$, 46, 63 neurons for olfactory bulb, aPC and pPC, respectively). Error bars represent s.e.m. based on the binomial model. Dashed lines inside the bars represent the FDRs resulting in only ~8% of order-sensitive cases in all three brain areas. (**g**) Percentage of order-sensitive responses as a function of the distance between the spots. Error bars represent s.e.m. based on the binomial model. The fraction of asymmetric TTCs in piriform cortex did not depend on the distance between the two spots as far as 1 mm on the olfactory bulb surface, indicating that order-sensitive temporal interactions occur between glomeruli that are widely distributed in the olfactory bulb. This also indicates that order sensitivity was not a result of an artifact caused by activation of adjacent spots through scattered light. (**h**) Percentage of cases in which the response to lagged stimulation (either A→B or B→A) was significantly higher than the response to A and B. The results were obtained in terms of the number of spot pairs (white bars) and neurons (gray bars). Error bars represent s.e.m. based on the binomial model. Dashed lines inside the bars represent the FDRs. ***$P < 0.001$ (binomial test against trial-shuffled controls, $n = 76$, 114, 129 spot pairs).
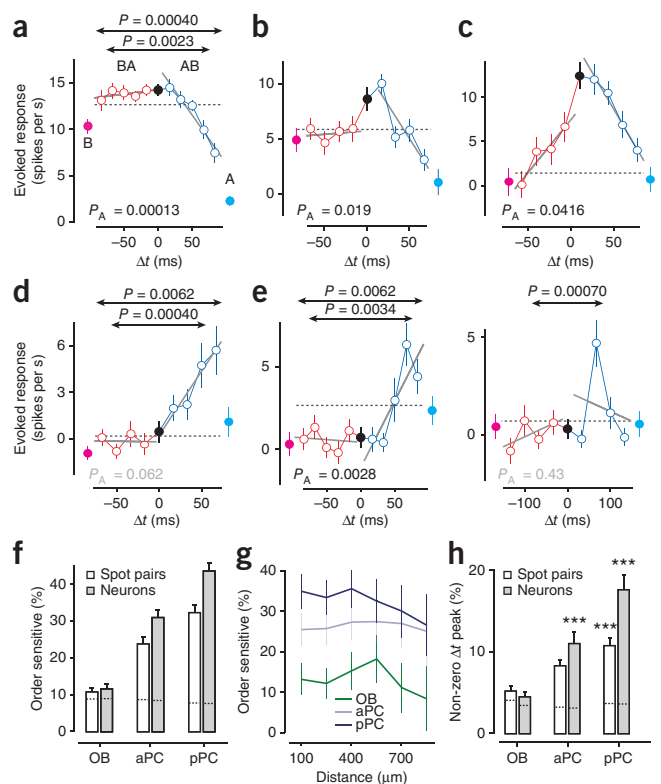
be explained if the activation of one spot, but not the other, causes delayed inhibition to the neuron (or its inputs) that suppresses the response to the second spot. In other cases, neurons did not respond to the second spot when the lag was longer than 50 ms in either order (**Fig. 5a**), suggesting that both spots reduced the responsiveness to later input. We found similar suppressive interactions in pairs of spots that were excitatory and neutral and in pairs that were excitatory and inhibitory (**Supplementary Fig. 8**).

To examine the time course of these delayed suppressive effects, we measured PCNs' responses with longer Δt (100–300 ms, 15 neurons, 35 responding cases). This experiment showed that even when an order-sensitive suppressive effect was found, such interaction diminished with longer lags (~200 ms; **Fig. 5b**). We counted the number of lag-specific asymmetries as a function of Δt over the population (**Fig. 5c**). The frequency of lag-specific asymmetry was higher with intermediate lags (~100 ms), and decreased to ~5% with larger lags ($\Delta t = 200$ and 300 ms) (similar to estimated FDR).

In addition to suppressive interactions, we observed TTCs with a nonzero peak, which is suggestive of lag-specific facilitations. These facilitatory interactions occurred not only when both spots

were excitatory (**Supplementary Fig. 8c**), but also when one or both spots were neutral (**Fig. 4d,e**).

These results suggest that delayed suppression, as well as excitation, is important for generating order sensitivity. In support of this idea, when a lag-specific difference was detected, the response of one of the orders was associated with supralinear (48% and 28%) or sublinear (26% and 47%) responses in both aPC and pPC, respectively (t test against $r(A) + r(B)$, $P < 0.05$, $n = 40$ repetitions; aPC, $n = 17$ spot pairs; pPC, $n = 29$ spot pairs; in which lag-specific difference was detected).

Firing rate–based coding versus relative time coding

We next examined the relative importance of specific neural codes (that is, temporal patterns versus firing rates) in conveying information about the relative timing of glomerular activations. We performed a decoding analysis, asking how accurately one can classify neural responses elicited by positive versus negative lags. We tested two types of temporal features of responses for temporal decoding: the rise time and the latency to the first spike. Consistent with the above results, in the olfactory bulb, decoding based on rate code performed poorly (~72% accuracy), whereas classification
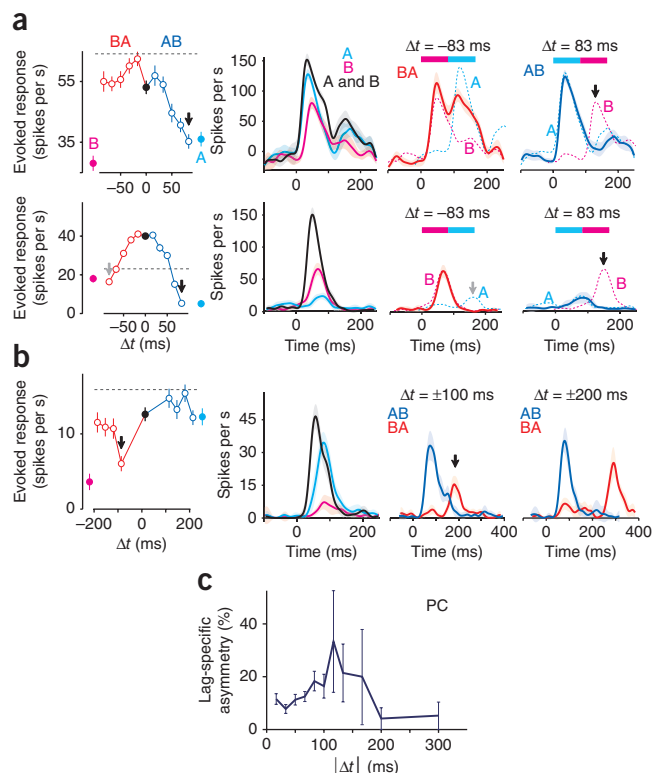
Figure 5 Delayed inhibition shapes the responsiveness of PCNs. (**a**) Top left, TTC of an example pPC neuron (shown in **Fig. 2d,h**). Top right panels, PETHs of the responses. The response decreased steeply with increasing Δt for A→B, but not for B→A. The dashed lines in the right two panels represent the expected firing rate changes in response to the corresponding spot (A or B). The second stimulation was effective in evoking responses with $\Delta t = -83$ ms (third panel), but not with $\Delta t = 83$ ms (fourth panel, black arrow). Bottom left, TTC of a pPC neuron. Bottom right panels, PETHs of the responses. With $\Delta t = \pm 83$ ms, the response to A→B differed significantly from that of B→A ($P = 4.5 \times 10^{-5}$, $t_{78} = 4.3$, t test). Note that second spot stimulation did not elicit the expected responses in both orders (middle and right panels, black and gray arrows). (**b**) TTC of a pPC neuron that was tested with longer lags ($\Delta t = 100$, 133, 167 and 200 ms). The TTC was asymmetric at $\Delta t = \pm 100$ ms (black arrow, $P = 2.3 \times 10^{-5}$, $t_{78} = 4.5$, t test, $n = 40$ repetitions), but similar for $\Delta t = 200$ ms ($P = 0.72$, t test, $t_{78} = 0.36$). With $\Delta t = -100$ ms, stimulation of the second spot A did not elicit a strong response (third panel, B→A, red line and black arrow). However, with a larger lag ($\Delta t = \pm 200$ ms), the response to spot A resumed (red line in the fourth panel). (**c**) Percentages of lag-specific asymmetry in TTCs for each lag for all PCNs. Data are presented as mean ± s.e.m. based on the binomial model.

These results indicate that information about relative timing of glomerular activations become available in the form of a firing rate–based code progressively more in aPC and pPC, whereas more peripheral areas convey the information with a timing-based code.

**The effect of respiration cycles and stimulation targets**

In this study, we focused on the effect of relative timing between neuronal activations. We therefore applied the optical stimulations randomly with respect to the respiration cycle, aiming to avoid confounds from the effect of timing with respect to respiration cycle. Nevertheless, *post hoc*, we analyzed whether the timing of optogenetic activations with respect to respiration cycle affected the shape of the TTCs and the magnitude of the response. Optogenetic stimulation activated neurons regardless of the phase of respiration cycle, although the magnitudes of response were modulated by the cycle (**Fig. 7a,b**). To examine whether the shape of TTCs depended on the time of light activation relative to the respiration cycle, we parceled the data into four mutually exclusive groups on the basis of the light-onset relative to the respiration cycle: groups with light onset that occurred during the first or second half of inhalation, and the first or second half of exhalation. This analysis revealed that the shapes of TTC were largely preserved across the different sniff phases (median Pearson correlation: 0.75–0.80 in PCNs; aPC, $n = 112$ TTCs; pPC, 95 TTCs; **Fig. 7c,d**). Firing rates were modulated to a greater extent in PCNs (when compared with OBNs) by the

based on the rise times performed well (~95%) (**Fig. 6a**). The high classification success rate using rise times is not surprising, as our stimulations differed only in the onset timing and relatively tight control of onset response in the olfactory bulb (**Fig. 2f** and **Supplementary Fig. 2**).

Notably, the classification success rates based on rate code increased in aPC (~78%) and increased further pPC (~92%). In contrast, the classification success rate in pPC based on rise times decreased to 82%, which was significantly lower than the success rate based on the rate code (~92%) ($P = 0.0001$, binomial test). Decoding based on latency to the first spike performed poorly in all brain regions and was lowest in pPC (62%). Considering only interacting spot pairs ($P < 0.05$, for both spots), the classification success rates based on rate code in the olfactory bulb decreased to ~50% and reached 95% in the pPC. The difference in classification success rates were more evident with increased numbers of spot pairs used in the analysis (**Fig. 6b**).

Figure 6 Rate code conveys relative timing information progressively more at the central areas. (**a**) Classification success rates based on three different decoding methods. A linear classifier was trained to classify the neuronal responses of a population of neurons as belonging to either positive or negative Δt. A classifier was first trained using all but 10% of the trials, including all Δt, and the remaining 10% of the trials were used to test the performance of the classifier (a leave-10%-out procedure). The result was obtained using neural activity representing 100 spot pairs randomly sampled from the data obtained from 45, 47 and 63 neurons in olfactory bulb (OB), aPC and pPC, respectively (see Online Methods). The mean classification success rate was obtained from 500 repetitions using different random sets of test trials. Rate code is based on the number of spikes evoked in the analysis window of 200 ms. Rise time code is based on the time at which the number of spikes in a window of 20 ms became ±2 s.d. higher (or lower) than the baseline. Latency to first spike time is defined as the time of the first spike from stimulation onset. *** $P < 0.001$ (binomial test). Data are presented as mean ± s.e.m. Dotted lines inside the bars represent the FDRs. (**b**) Classification success rates as a function of the number of spot pairs. Data are presented as mean ± s.e.m. ($n = 500$ repeats). The lower and upper dotted horizontal lines represent the minimum and maximum FDRs.
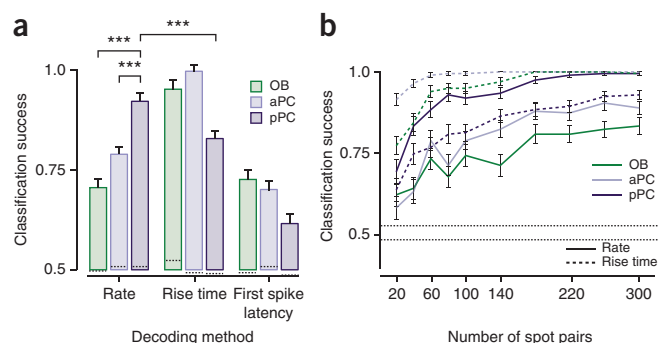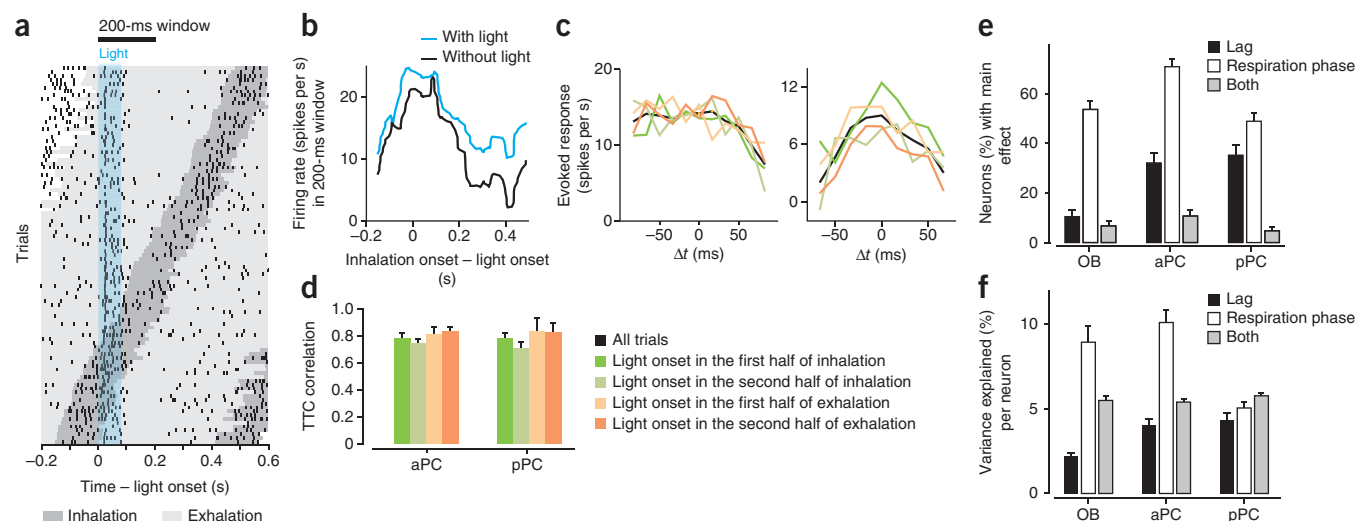
Figure 7 Order selectivity is largely preserved across different respiration phases. (**a**) Raster plot of a mitral and tufted cell in response to single spot optical stimulation. Each tick mark represents one spike. The dark gray areas indicate inhalation periods and the light gray areas indicate exhalation periods. Trials are sorted by the timing of inhalation onset. The timing of light stimulation (duration = 83 ms) is indicated by the cyan area. This neuron fired preferentially during inhalation periods. (**b**) Firing rates in a 200-ms window (indicated at the top of **a**) as a function of inhalation onset timing relative to light onset (cyan). The data with no light stimulation (black) was obtained by randomly assigning light onset relative to the respiration cycle. (**c**) Two examples comparing TTCs at specific respiration phases. The data were parceled into four groups depending on the onset of light stimulation (as indicated in **d**). The shapes of TTCs were similar across the four groups. (**d**) Correlation of TTCs. A TTC was obtained for each of the four groups, as in **c**. The correlation between this TTC and the TTC computed with all other trial groups was obtained. The bar graphs show the median correlation across all spot pairs in each brain area. TTCs were obtained only if at least ten trials were available for all of the four groups (aPC, $n = 112$ TTCs; pPC, 95 TTCs). Data are presented as mean ± s.d. (**e**) Percentage of neuron spot pairs that were modulated by the lag and/or the respiration phase (two-way ANOVA, $F_{3,199} > 2.6$ and/or $F_{4,199} > 2.4$, $P < 0.05$, for 4 and 5 Δt, respectively, uncorrected for multiple comparisons). Many neurons were modulated by the respiration phase (white bars). Many neurons in aPC and pPC were modulated by the lag between two spot activations, but neurons in olfactory bulb were not (black bars; binomial test, $P < 0.001$ for both aPC and pPC compared to olfactory bulb). Error bars represent s.e.m. based on the binomial model. The number of TTCs used in the analysis was 134, 224 and 190 in the olfactory bulb, aPC and pPC, respectively. (**f**) The variance of neural responses explained by different factors per neuron (two-way ANOVAs, the average variance explained by the lag, respiration phase or both). Respiration phase explains on average ~10% of the variance in olfactory bulb and aPC. The lag between spot activations explain more of the variance in PCNs than in OBNs (aPC, $Z = -3.2$, $P = 0.0011$; pPC, $Z = -4.3$, $P = 0.000016$; compared with olfactory bulb, Mann-Whitney U test). Data are presented as mean ± s.e.m. ($n = 134$, 224 and 190 TTCs in the olfactory bulb, aPC and pPC, respectively).

lag between the two spot stimulations than by its timing with respect to the respiration cycle (two-way ANOVA; **Fig. 7e,f**).

To examine whether the temporal sensitivity found above depends on 'pre–mitral and tufted' processing, we generated transgenic mice expressing ChR2 specifically in mitral and tufted cells (*Tbet* (also known as *Tbx21*)-*cre; ChR2^loxP/loxP^* mice; **Fig. 8a,b** and **Supplementary Fig. 9**). This allowed us to directly activate mitral and tufted cells,

bypassing some of the pre–mitral and tufted cell interactions. Similar to the above results, PCNs were sensitive to relative timing of mitral and tufted cell activations (piriform cortex, 33%; olfactory bulb, 13%; **Fig. 8c**). These results suggest that interactions presynaptic to mitral and tufted cells do not have a major role in the generation of order sensitivity and that temporal interactions occur largely between mitral and tufted cells and the piriform cortex.

Figure 8 Direct activation of mitral and tufted cells produced consistent results. (**a**) Experimental design. Data are presented as in **Figure 1a**. (**b**) Characterization of *Tbet-cre; ChR2^loxP/loxP^* mouse. Left, a section from a *Tbet-cre; LacZ^loxP/loxP^* mouse. Blue signals (LacZ staining) depict the location of cell bodies. Mitral and tufted cells (arrowheads) are stained. Right, fluorescent image of an olfactory bulb section. Red indicates the location of ChR2 tagged with a red fluorescent protein (tdTomato). Sections from $n = 2$ and $n > 20$ mice were examined for LacZ staining and tdTomato fluorescence, respectively.

EPL, external plexiform layer; GL, glomerular layer; GCL, granule cell layer; MCL, mitral cell layer; OB, olfactory bulb. Scale bar represents 100 μm. (**c**) Percentage of order-sensitive responses in olfactory bulb ($n = 17$ neurons and 28 responding spot pairs) and PCNs ($n = 34$ neurons and 67 responding spot pairs). The results were obtained in terms of spot pairs (white bars) and neurons (gray bars). The data from aPC and pPC were pooled. Dashed lines inside the bars represent the FDRs. Error bars represent s.e.m.
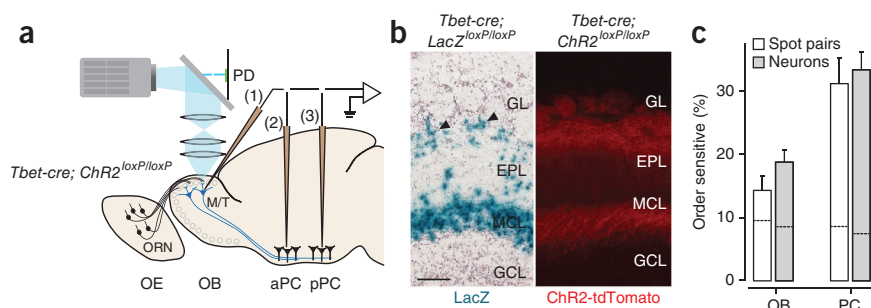
DISCUSSION

We examined whether neurons in the olfactory system are sensitive to changes in temporal patterns of activation in the olfactory bulb. We found that activating multiple glomeruli with different relative timing on a timescale of tens of milliseconds elicited distinct firing-rate responses in PCNs, but only rarely did so in mitral and tufted cells in the olfactory bulb. Notably, we found that PCNs were sensitive to the order and the lag of glomerular activation. Furthermore, pPC neurons were more sensitive than aPC neurons. Order-sensitive interactions in PCNs occurred frequently for paired glomerular activation, regardless of the separating distance (up to ~1 mm). It has been postulated that odor information is encoded by the identity and a combination of activated glomeruli, or their spatial patterns[33,34], and that PCNs detect specific combinations of glomerular activations[19,20]. Our findings indicate that, in addition to identity or spatial codes, the relative timing of glomerular activation constitutes an important part of an odor code in the olfactory bulb.

Coincidence or sequence detection

A previous study in zebrafish showed that neurons in the posterior zone of the dorsal telencephalon effectively discard information about synchrony in the olfactory bulb as a result of long membrane time constants of dorsal telencephalon neurons and relatively weak feedforward inhibition in dorsal telencephalon[13]. In contrast, we found that, in many PCNs, simultaneous stimulation of two olfactory bulb foci caused larger activation than non-simultaneous stimulation. This apparent inconsistency may be a result of the differences in light stimulation parameters (for example, durations), but may also be a result of the prominent feedforward inhibition in the mammalian piriform cortex that shortens the temporal integration window[18].

Odor stimulation activates individual mitral and tufted cells in the olfactory bulb with odor- and neuron-specific temporal patterns. As a result, ensemble activity patterns evolve over time, forming an odor-specific 'trajectory' in a multi-dimensional neuron space[12,35]. It has been proposed that downstream neurons read out the instantaneous activity patterns of inputs in a short time window (~50 ms) because high-frequency oscillations 'chunk' each oscillation cycle into a unit of information[36]. According to this view, preceding input patterns or trajectories do not affect the response of downstream neurons. In contrast, we found that PCNs' responses were greatly affected by the preceding patterns of glomerular activation (up to ~200 ms), suggesting that PCNs can read out the entire trajectory and act as sequence detectors.

Relative time code

Discussing temporal coding requires a definition of a reference point to which spikes are aligned. Previous studies have used the timing from the onset of inhalation[9,10,12,37]. The sniff phase has also been proposed as a better reference, as the fidelity of spike timing is improved when aligned to the sniff phase[11] (but see refs. 12,37). An alternative scheme is to use relative timing across multiple neurons[38,39]. In this scheme, a reference defined by an external factor (for example, respiration) is not required. Relative time codes may have computational advantages[5,38,39]. Our finding that TTCs are preserved across stimulations occurring at different respiration phases supports the robustness of relative timing–based coding.

A recent study examined whether mice can discriminate the timing of ORN stimulations with respect to the respiration cycle (sniff phase)[14]. This study, however, was not able to examine the role of relative timing, as the same ORN population was activated at different times relative to inhalation onset. In contrast, we found that PCNs can read out pure timing differences in the olfactory bulb.

Mechanisms

The piriform cortex contains prominent feedforward, as well as feedback (recurrent), inhibition[18,29–32]. Feedforward inhibition is activated by direct mitral and tufted cell inputs, has short latency (<10 ms), quickly decays during trains of activations, and is thought to involve GABA neurons in the outermost layer[29,30]. Feedback inhibition requires the activation of principal cells in piriform cortex, which may require stronger mitral and tufted cell inputs. As a consequence, feedback inhibition has late onset (tens of milliseconds) and likely involves fast-spiking GABA neurons in the deep layer[29–31]. We found that order-sensitive responses were most frequently observed with a lag of ~100 ms, and that, in many of these cases, excitatory responses to the second spot were suppressed by the activation of the first spot (**Fig. 5a,b** and **Supplementary Figs. 8a,b** and **10**). Notably, these inhibitory interactions occurred after the activation of an excitatory, neutral or inhibitory spot, and were spot pair specific (that is, not completely 'global'). In addition, although single spot stimulation caused inhibitory responses more frequently in the olfactory bulb, we found very little order sensitivity in the olfactory bulb, indicating that not all kinds of inhibition generate order sensitivity.

In addition to inhibitory interactions, the existence of supralinear interactions suggests that nonlinear excitatory interactions may be important for generating order sensitivity. In addition to monosynaptic excitatory inputs from mitral and tufted cells[40–43], PCNs receive polysynaptic excitatory inputs from mitral and tufted cells through recurrent (association) connections from its local, as well as other, cortical areas. Recurrent excitation can cause excitation at various delays (~10–70 ms[40,44]; **Supplementary Fig. 8d**). Thus, when a PCN receives monosynaptic and delayed, polysynaptic inputs, detecting coincidence of these inputs allows it to respond preferentially to a specific lag between them. Such a mechanism could explain a peak at a nonzero lag (**Fig. 4d,e** and **Supplementary Fig. 8c**). Furthermore, more prominent recurrent connections exist in pPC than in aPC[40,43], consistent with our observation that pPC neurons were more sensitive to orders than aPC neurons. Furthermore, short-term synaptic plasticity[16,45,46] or biophysical properties of single neurons, such as nonlinear dendritic integration that can facilitate discrimination of temporal orders of different inputs[47] (but see ref. 48), may be important for generating order sensitivity.

Finally, although optogenetic stimulation of olfactory nerve input caused relatively tight onset responses, the duration and magnitude of activation varied across mitral and tufted cells (**Supplementary Fig. 2**), as observed during odor stimulation. The difference in magnitude and time course can be a result of the variability in cellular and network properties, such as the strengths of synaptic connections between olfactory nerve and mitral and tufted cells, spiking thresholds and temporal filtering properties of mitral and tufted cells[49,50], as well as the difference in lateral- and self-inhibitory interactions. Thus, it is possible that asymmetric TTCs were generated in part because excitatory periods of mitral and tufted cells overlap in one order of stimulation, but not the other. This mechanism may be involved in converting relative timing of the olfactory nerve activations into different firing-rate responses in PCNs.

How the brain processes differences in the timing of spikes is a general problem in sensory physiology. To better understand this question, it is imperative to understand the mechanisms that serve to encode, and then later decode, sensory input. Previous studies have largely focused on the mechanisms that serve to encode such input. However, a deeper understanding of the decoding problem will be indispensable for a full understanding of how a particular

neural code works in neural circuits. The use of optogenetics, as done in the present study, provides a unique ability to examine the latter, decoding problem.

METHODS

Methods and any associated references are available in the online version of the paper.

Note: Supplementary information is available in the online version of the paper.

AUTHOR CONTRIBUTIONS

R.H. and N.U. conceived the experiment. R.H. performed the experiment. A.L. generated and characterized the *Tbet-cre; ChR2^{loxP/loxP}* mice, and L.M. and H.Z. generated and characterized the *ChR2^{loxP/loxP}* mice. V.N.M. provided the *Omp-ChR2* mice. R.H. and N.U. wrote the paper and A.L., V.N.M. and H.Z. provided feedback on the manuscript.

COMPETING FINANCIAL INTERESTS

The authors declare no competing financial interests.

Reprints and permissions information is available online at http://www.nature.com/reprints/index.html.

1. Adrian, E.D. The impulses produced by sensory nerve endings: part I. *J. Physiol.* (*Lond.*) **61**, 49–72 (1926).
2. Wehr, M. & Laurent, G. Odour encoding by temporal sequences of firing in oscillating neural assemblies. *Nature* **384**, 162–166 (1996).
3. VanRullen, R., Guyonneau, R. & Thorpe, S.J. Spike times make sense. *Trends Neurosci.* **28**, 1–4 (2005).
4. Laurent, G. A systems perspective on early olfactory coding. *Science* **286**, 723–728 (1999).
5. Hopfield, J.J. Pattern recognition computation using action potential timing for stimulus representation. *Nature* **376**, 33–36 (1995).
6. Spors, H. & Grinvald, A. Spatio-temporal dynamics of odor representations in the mammalian olfactory bulb. *Neuron* **34**, 301–315 (2002).
7. Wesson, D.W., Carey, R.M., Verhagen, J.V. & Wachowiak, M. Rapid encoding and perception of novel odors in the rat. *PLoS Biol.* **6**, e82 (2008).
8. Macrides, F. & Chorover, S.L. Olfactory bulb units: activity correlated with inhalation cycles and odor quality. *Science* **175**, 84–87 (1972).
9. Cang, J. & Isaacson, J.S. *In vivo* whole-cell recording of odor-evoked synaptic transmission in the rat olfactory bulb. *J. Neurosci.* **23**, 4108–4116 (2003).
10. Margrie, T.W. & Schaefer, A.T. Theta oscillation coupled spike latencies yield computational vigor in a mammalian sensory system. *J. Physiol.* (*Lond.*) **546**, 363–374 (2003).
11. Shusterman, R., Smear, M.C., Koulakov, A.A. & Rinberg, D. Precise olfactory responses tile the sniff cycle. *Nat. Neurosci.* **14**, 1039–1044 (2011).
12. Cury, K.M. & Uchida, N. Robust odor coding via inhalation-coupled transient activity in the mammalian olfactory bulb. *Neuron* **68**, 570–585 (2010).
13. Blumhagen, F. *et al.* Neuronal filtering of multiplexed odor representations. *Nature* **479**, 493–498 (2011).
14. Smear, M., Shusterman, R., O'Connor, R., Bozza, T. & Rinberg, D. Perception of sniff phase in mouse olfaction. *Nature* **479**, 397–400 (2011).
15. Miura, K., Mainen, Z.F. & Uchida, N. Odor representations in olfactory cortex: distributed rate coding and decorrelated population activity. *Neuron* **74**, 1087–1098 (2012).
16. Kadohisa, M. & Wilson, D.A. Olfactory cortical adaptation facilitates detection of odors against background. *J. Neurophysiol.* **95**, 1888–1896 (2006).
17. Stettler, D.D. & Axel, R. Representations of odor in the piriform cortex. *Neuron* **63**, 854–864 (2009).
18. Luna, V.M. & Schoppa, N.E. GABAergic circuits control input-spike coupling in the piriform cortex. *J. Neurosci.* **28**, 8851–8859 (2008).
19. Apicella, A., Yuan, Q., Scanziani, M. & Isaacson, J.S. Pyramidal cells in piriform cortex receive convergent input from distinct olfactory bulb glomeruli. *J. Neurosci.* **30**, 14255–14260 (2010).
20. Davison, I.G. & Ehlers, M.D. Neural circuit mechanisms for pattern detection and feature combination in olfactory cortex. *Neuron* **70**, 82–94 (2011).
21. Dhawale, A.K., Hagiwara, A., Bhalla, U.S., Murthy, V.N. & Albeanu, D.F. Non-redundant odor coding by sister mitral cells revealed by light addressable glomeruli in the mouse. *Nat. Neurosci.* **13**, 1404–1412 (2010).
22. Arenkiel, B.R. *et al. In vivo* light-induced activation of neural circuitry in transgenic mice expressing channelrhodopsin-2. *Neuron* **54**, 205–218 (2007).
23. Carey, R.M., Verhagen, J.V., Wesson, D.W., Pirez, N. & Wachowiak, M. Temporal structure of receptor neuron input to the olfactory bulb imaged in behaving rats. *J. Neurophysiol.* **101**, 1073–1088 (2009).
24. Wachowiak, M. All in a sniff: olfaction as a model for active sensing. *Neuron* **71**, 962–973 (2011).
25. Uchida, N. & Mainen, Z.F. Speed and accuracy of olfactory discrimination in the rat. *Nat. Neurosci.* **6**, 1224–1229 (2003).
26. Davison, I.G. & Katz, L.C. Sparse and selective odor coding by mitral/tufted neurons in the main olfactory bulb. *J. Neurosci.* **27**, 2091–2101 (2007).
27. Nagayama, S., Takahashi, Y.K., Yoshihara, Y. & Mori, K. Mitral and tufted cells differ in the decoding manner of odor maps in the rat olfactory bulb. *J. Neurophysiol.* **91**, 2532–2540 (2004).
28. Benjamini, Y. & Hochberg, Y. Controlling the false discovery rate: a practical and powerful approach to multiple testing. *J. R. Stat. Soc. Series B Stat. Methodol.* **57**, 289–300 (1995).
29. Stokes, C.C. & Isaacson, J.S. From dendrite to soma: dynamic routing of inhibition by complementary interneuron microcircuits in olfactory cortex. *Neuron* **67**, 452–465 (2010).
30. Suzuki, N. & Bekkers, J.M. Microcircuits mediating feedforward and feedback synaptic inhibition in the piriform cortex. *J. Neurosci.* **32**, 919–931 (2012).
31. Satou, M., Mori, K., Tazawa, Y. & Takagi, S.F. Interneurons mediating fast postsynaptic inhibition in pyriform cortex of the rabbit. *J. Neurophysiol.* **50**, 89–101 (1983).
32. Poo, C. & Isaacson, J.S. Odor representations in olfactory cortex: "sparse" coding, global inhibition, and oscillations. *Neuron* **62**, 850–861 (2009).
33. Buck, L.B. The molecular architecture of odor and pheromone sensing in mammals. *Cell* **100**, 611–618 (2000).
34. Mori, K. & Sakano, H. How is the olfactory map formed and interpreted in the Mammalian brain? *Annu. Rev. Neurosci.* **34**, 467–499 (2011).
35. Stopfer, M., Jayaraman, V. & Laurent, G. Intensity versus identity coding in an olfactory system. *Neuron* **39**, 991–1004 (2003).
36. Perez-Orive, J. *et al.* Oscillations and sparsening of odor representations in the mushroom body. *Science* **297**, 359–365 (2002).
37. Carey, R.M. & Wachowiak, M. Effect of sniffing on the temporal structure of mitral/tufted cell output from the olfactory bulb. *J. Neurosci.* **31**, 10615–10626 (2011).
38. Junek, S., Kludt, E., Wolf, F. & Schild, D. Olfactory coding with patterns of response latencies. *Neuron* **67**, 872–884 (2010).
39. Schaefer, A.T. & Margrie, T.W. Spatiotemporal representations in the olfactory system. *Trends Neurosci.* **30**, 92–100 (2007).
40. Haberly, L.B. Summed potentials evoked in opossum prepyriform cortex. *J. Neurophysiol.* **36**, 775–788 (1973).
41. Franks, K.M. *et al.* Recurrent circuitry dynamically shapes the activation of piriform cortex. *Neuron* **72**, 49–56 (2011).
42. Poo, C. & Isaacson, J.S. A major role for intracortical circuits in the strength and tuning of odor-evoked excitation in olfactory cortex. *Neuron* **72**, 41–48 (2011).
43. Hagiwara, A., Pal, S.K., Sato, T.F., Wienisch, M. & Murthy, V.N. Optophysiological analysis of associational circuits in the olfactory cortex. *Front. Neural Circuits* **6**, 18 (2012).
44. Mouly, A.M., Litaudon, P., Chabaud, P., Ravel, N. & Gervais, R. Spatiotemporal distribution of a late synchronized activity in olfactory pathways following stimulation of the olfactory bulb in rats. *Eur. J. Neurosci.* **10**, 1128–1135 (1998).
45. Oswald, A.M. & Urban, N.N. Interactions between behaviorally relevant rhythms and synaptic plasticity alter coding in the piriform cortex. *J. Neurosci.* **32**, 6092–6104 (2012).
46. Suzuki, N. & Bekkers, J.M. Neural coding by two classes of principal cells in the mouse piriform cortex. *J. Neurosci.* **26**, 11938–11947 (2006).
47. Branco, T., Clark, B.A. & Hausser, M. Dendritic discrimination of temporal input sequences in cortical neurons. *Science* **329**, 1671–1675 (2010).
48. Bathellier, B., Margrie, T.W. & Larkum, M.E. Properties of piriform cortex pyramidal cell dendrites: implications for olfactory circuit design. *J. Neurosci.* **29**, 12641–12652 (2009).
49. Padmanabhan, K. & Urban, N.N. Intrinsic biophysical diversity decorrelates neuronal firing while increasing information content. *Nat. Neurosci.* **13**, 1276–1282 (2010).
50. Angelo, K. *et al.* A biophysical signature of network affiliation and sensory processing in mitral cells. *Nature* **488**, 375–378 (2012).

ONLINE METHODS

Animal preparation. All surgical and experimental procedures were in accordance with the US National Institutes of Health Guide for the Care and Use of Laboratory Animals and approved by the Harvard Institutional Animal Care and Use Committee. Mice (both males and females, 3–6 months old) were housed in a group in a cage in a reverse light/dark cycle, and all experiments were performed during their dark cycle. Mice had not received any experimental treatment except genotyping. All mice were backcrossed with C57BL/6J. No mice were excluded after the experiment.

We used a transgenic mouse line in which ChR2 is expressed under the control of the olfactory marker protein gene (*Omp-ChR2* mice[21], *n* = 34 mice). We also used mice that express ChR2 specifically in mitral and tufted cells (*Tbet-cre; ChR2*[loxP/loxP] mice, *n* = 11 mice). These mice were obtained by crossing a transgenic mouse line, Tg(Tbet-cre), that expresses Cre recombinase under the control of the *Tbet* gene (*Tbet-cre*) and Ai27D (B6.Cg-Gt(ROSA)26Sor[tm27.1(CAG-COP4*H134R/tdTomato)Hze/J]), a knock-in mouse line that conditionally expresses a ChR2/tdTomato fusion protein from the *Gt(ROSA)26Sor* locus[51].

Tg(Tbet-cre) mice were generated using a BAC transgenic approach. Specifically, *cre* cDNA (pSP13-Cre) sequences were recombined at the start ATG of the *Tbet* gene on BAC RP23-237M14 (ref. 52). The *Tbet-cre* expression pattern was determined through crosses to three independent conditional reporter lines (Rosa26-lsl-lacz, rosa26-lsl-tdTomato, and Rosa26-lsl-ChR2-tdTomato). Multiple mice in each background were analyzed (*n* = 2, *n* > 20 and *n* > 20 mice, respectively; **Fig. 8** and **Supplementary Fig. 9**).

Mice were anesthetized with ketamine (60 mg per kg of body weight) and medetomidine (0.5 mg per kg, intraperitoneal), fixed in a stereotaxic frame, and the bone overlying the dorsal olfactory bulb was removed. In some experiments, another craniotomy was made above the aPC or pPC (aPC, ~2 mm anterior from bregma, ~2 mm lateral from midline; pPC, ~1 mm posterior from bregma, ~3.5 mm lateral from midline). Additional anesthesia was administrated as necessary (~30% of original dose). The mice's body temperature was maintained at 37 °C using a homeothermic blanket system.

Electrophysiology. Spiking activities of neurons were recorded extracellularly using a tungsten electrode (~10 MΩ). Neural signals were amplified and filtered at 300–3,000 Hz (CyberAmp-380, Axon Instruments). During recording from piriform cortex, the recording site was verified on the basis of the waveforms evoked by wide-field optical stimulation of the olfactory bulb (duration = 17 ms), which caused stereotypical evoked responses similar to electrical stimulation of lateral olfactory tract[40]. Further verification was performed on the basis of histology. Respiration was monitored using a thermocouple placed in front of the nose[25]. The recording locations were not blinded to the experimenters.

Spike signals were sorted offline using MClust software in MATLAB (written by A.D. Redish, University of Minnesota). Only well-isolated neurons that met the following two criteria were used: the mean amplitude of spikes was larger than 5 s.d. of the voltage signal, and the number of spikes with an interspike interval below 3 ms (the refractory period) was less than 5%.

Good isolation of selected neurons was further confirmed using a metric for cluster separation (L-ratio[53]): 91% of recorded neurons had an L-ratio smaller than 0.05. The main result of our analysis does not change qualitatively if we consider all neurons, or if we remove neurons in which the number of spikes with interspike interval below 3 ms was more than 2% of the total spikes.

Optical stimulation of the olfactory bulb. We used a digital light processing projector (TXR774, Optoma; frame rate = 60 Hz). A system of three lenses was employed to project minified images on the olfactory bulb (**Fig. 1a**). One single-lens (SLR) photo lens (Nikon 50 mm f/1.4, AF) was placed after a dichroic mirror (DMLP425R, Thorlabs). Two photo lenses (FL, 150-mm and 75-mm achromatic doublet, Thorlabs) were used to focus and minimize the image onto the olfactory bulb. At this minification, one pixel of a projected image corresponded to ~10 μm. To get a timestamp of the light stimulus, we used a photodiode (FDS1010, 400-ns rise time, Thorlabs) to detect stray excitation light that bled through the dichroic mirror. Optical stimulation was controlled with the MATLAB psychophysical toolbox (http://psychtoolbox.org/). The number of repeats for a given condition was typically 40.

The total area scanned for each experiment was determined by the size of craniotomy. In most experiments, we used square spots of ~150 μm. Thus, it is

likely that we activated one to several glomeruli. In a smaller number of cases, we tested temporal sensitivity using spots of smaller (~80–100 μm) or larger (~200 μm) auW. No substantial difference was found and we therefore pooled all data. The light intensity used was accommodated to get a moderate response and ranged between 10–30 mW mm^{-2} as measured using a photometer.

We cannot exclude the possibility that optical stimulation activated fibers of passage outside a focal spot containing glomeruli. However, it is unlikely that our conclusions are affected by this effect. First, glomeruli have an order of magnitude higher sensitivity than fibers of passage[21]. Indeed, only 4% of the spots outside a focal point elicited statistically significant excitation in mitral and tufted cells (*t* test, *P* < 0.05, *n* = 20 repetitions, 1,352 tested spots; estimated FDR = 5.3%). Similarly, the number of spot pairs in which both spots excited a mitral and tufted cell was 5% in the *Omp-ChR2* mice, and 0% in the *Tbet-cre* mice. These results indicate that activation of mitral and tufted cells by activating fibers of passage in the *Omp-ChR2* mice was minimal. Second, we obtained similar results using *Tbet-cre* mice in which ChR2 was not expressed in olfactory nerve fibers. Third, our main conclusion that PCNs are sensitive to the timing of glomerular activations does not require that we stimulate only one glomerulus.

Data set. Each neuron was typically tested with three spots that make up of three spot pairs (3.0 ± 1.6 pairs per neuron, mean ± s.d.). Before selecting spot pairs, we performed mapping with single spot stimulations (3–10 repetitions per spot), and identified candidate excitatory and inhibitory spots. Two or three spots were chosen randomly except that we tried to include at least one excitatory spot for each neuron. In *Omp-ChR2* mice, we tested 112, 152 and 191 spot pairs from 45, 47 and 63 neurons in olfactory bulb, aPC and pPC, respectively (*n* = 17, 11 and 14 mice). About 30% of the spot pairs did not show a significant response in any of the stimulus conditions (*t*-test against baseline, *P* < 0.05 divided by the number of lags tested), and these spot pairs were excluded from the analysis. As a result, the main data set using *Omp-ChR2* mice consisted of 76, 114 and 129 TTCs obtained from the olfactory bulb, aPC and aPC, respectively. The results were qualitatively the same when we repeated the analyses without removing non-responsive spot pairs. We chose these sample numbers on the basis of comparable studies in the field[20,41] and on our observation that similar results were obtained with about a half sample size of that used in the main analyses.

In *Tbet-cre; ChR2*[loxP/loxP] mice, we tested 48, 65 and 27 spot pairs from 17, 23 and 11 neurons in the olfactory bulb, aPC and pPC, respectively (*n* = 5, 5 and 3 mice). About 32% of the spot pairs did not show any response and were excluded from the analysis. The main data set using *Tbet-cre; ChR2*[loxP/loxP] mice consists of 28, 46 and 21 TTCs in olfactory bulb, aPC and pPC, respectively. The results were qualitatively the same when we repeated the analyses without removing non-responsive spot pairs. Single spot scanning experiments (**Fig. 1**) were performed on 29, 25 and 22 neurons recorded from olfactory bulb, aPC and pPC neurons in *Omp-ChR2* mice, independently from the above data set. Experiments with repeated stimulations of a single spot were performed on 8, 8 and 6 neurons in olfactory bulb, aPC and pPC in *Omp-ChR2* mice. The sample sizes for *Tbet-cre* mice were about the half of those in the main data set. This was sufficient to statistically demonstrate that the results obtained in both data sets were similar.

Data analysis. All values are represented as mean ± s.e.m. unless otherwise noted. All statistical tests were conducted with a nonpaired, two-sided *t* test unless stated otherwise. When the normality assumption was not valid, we used the Mann-Whitney *U* test.

To obtain neural responses, we used a fixed time window of the duration of 200 ms. The start time of the analysis window was adjusted for each brain area to accommodate for the transduction delays (10 ms in mitral and tufted cells, 25 ms for PCNs from the onset of the first light). A response was defined as a firing rate change from the baseline (a window of 0–200 ms before light onset). PETHs were smoothed using a Gaussian filter (s.d. = 15 ms).

For the analysis of one spot stimulations (**Supplementary Fig. 2**), latency is defined as the time at which the firing rate in a window of 20 ms was significantly higher (*P* < 0.05) or lower than the firing rate in a 200-ms window before stimulation onset. We used all of the neurons in which we found a significant activation (*P* < 0.05, *t* test).

To quantify the TTCs shape in a population of OBNs and PCNs, we fitted a line to the TTCs for the positive and negative Δ*t* separately. The fitting was done using

the absolute value of Δt (that is, |Δt|) as the independent variable. The results were similar when fitting was performed without including the point of Δt = 0.

To determine whether TTCs were flatter in OBNs than in PCNs, we performed additional analyses. First, we performed the ANOVA with the lags between the spot stimulations as the main factor. We then compared the distributions of the obtained P values between areas, which revealed that OBNs generally had larger P values (**Supplementary Fig. 4c,d**), supporting the idea that neural responses were flatter in OBNs.

Second, we compared the following models fitted to the firing rate data: $r = b$ (model 1), $r = b_{\Delta t}$ (model 2) and $r = b + a\Delta t$ (model 3, fitted for positive and negative t separately), where r is the neural responses, Δt is the lag, and a and b are constants, and $b_{\Delta t}$ is a constant defined for each Δt. Our prediction was that, if neural responses were not modulated by the lag, we should observe a small improvement using models 2 or 3 compared with model 1. We quantified the goodness of fit using the mean square errors and the improvement using the difference in mean square errors using two models. Larger improvements were observed for PCNs than for OBNs (**Supplementary Fig. 4e,f**).

The ANCOVA was performed without including the simultaneous stimulations condition (Δt = 0) and without considering the significance of the fitted lines. However, the results were similar when it was performed using the Δt = 0 condition and/or when we considered only cases in which the fitted lines were significantly valid (both slope and intercept, $P < 0.05$).

To quantify the magnitude of lag-specific differences without relying on a specific P value threshold test, we computed the area under the receiver-operating characteristic curve between the two firing rate distributions for each Δt. The area under the receiver-operating characteristic curve quantifies the degree of overlap (that is, discriminability) between two distributions. This analysis showed that lag-specific differences between positive and negative Δt were larger in the pPC and aPC than in the olfactory bulb ($P < 0.001$ for both aPC and pPC, Kolmogorov-Smirnov test; **Supplementary Fig. 6d**). We also compared the firing rates for positive and negative Δt by pooling all Δt separately for positive and negative Δt (t test, $P < 0.05$). This analysis also produced similar results (4.2, 14.3 and 22.3% in olfactory bulb, aPC and pPC, respectively; 3–5% FDRs).

To estimate the FDRs using the two criteria for detecting asymmetric TTCs, we performed a trial-shuffled control analysis[28]. The firing rate data for each spot pair were shuffled with respect to Δt to obtain a surrogate data. Shuffling was performed 30 times to obtain the average FDR.

We also calculated the fraction of neurons that had at least one spot pair that had an asymmetric TTC (Bonferroni correction with both the numbers of spot pairs and the lags). Again, the fraction of neurons that had asymmetric TTCs was significantly highest in pPC (43%, $P = 0.02$, and $P < 0.001$ for pPC versus aPC and pPC versus olfactory bulb, respectively, binomial test; **Fig. 4f**).

Mitral and tufted cells' response to light stimulation increased linearly with light intensity without apparent saturation with the range of light intensity used (**Supplementary Fig. 2j,k**). To further characterize the time course of delayed suppression, we measured responses of OBNs and PCNs to repeated stimulations of a single spot applied with different lags. PCNs' responses to the second stimulation were often suppressed by the first stimulation (**Supplementary Fig. 10d–f**). Suppression was stronger in PCNs than in OBNs (t test, $P < 0.001$, $n = 40$ repetitions at Δt = 166 ms in OBNs and PCNs, **Supplementary Fig. 10c,f**). The median response of the normalized responses in piriform cortex was lower than that in olfactory bulb for all lags tested (significantly lower up to lags of 500 ms, $Z > 2.5$, $P < 0.05$, Mann-Whitney U test, $n = 40$ repetitions). Since the reduction in PCNs was larger than those in OBNs, it could not be attributed solely to ChR2 desensitization[54].

For classification analysis, the trials were classified into two categories, positive and negative Δt values. We used spot pairs pooled across all experiments. Input to the algorithm consisted of activity vectors derived from single-trial responses, where the length of the vector was determined by the number of spot pairs. To compute classification success, 10% of trials were chosen as a test set, and the remaining trials were used to train the algorithm. Classification was performed based on the distance (Pearson correlation) between the test trials and the average response vector obtained from the training trials. The test trials were averaged to construct one representative test vector and compared with the average of the remaining positive and negative training trials. Test trials were selected randomly from each neuron spot pair. For firing rate–based classification, we used the firing rate in a 200-ms window after light onset. For the rise time code we used the time at which the number of spikes in a 20-ms window was 2 s.d. higher (or lower) than the baseline. The average and s.d. of spontaneous spikes (baseline) was calculated using ten 20-ms time windows in the 200-ms window before light onset. Latency to first spike is defined as the time of first spike from light onset. To generate a vector of a given number of spot pairs, we randomly down- or up-sampled the data (**Fig. 5b**).

The control experiments using reduced light conditions were performed using OMP-ChR2 mice ($n = 5$ mice, 34 neurons, 34 TTCs) and *Tbet-cre* mice ($n = 1$ mice, 11 neurons, 11 TTCs). When we quantified the accuracy with which one can classify positive versus negative Δt in this mitral and tufted cell population, the classification success rates remained low (62%, 45 spot pairs).

51. Madisen, L. *et al.* A toolbox of Cre-dependent optogenetic transgenic mice for light-induced activation and silencing. *Nat. Neurosci.* **15**, 793–802 (2012).
52. Yang, X.W., Model, P. & Heintz, N. Homologous recombination based modification in *Escherichia coli* and germline transmission in transgenic mice of a bacterial artificial chromosome. *Nat. Biotechnol.* **15**, 859–865 (1997).
53. Schmitzer-Torbert, N. & Redish, A.D. Neuronal activity in the rodent dorsal striatum in sequential navigation: separation of spatial and reward responses on the multiple T task. *J. Neurophysiol.* **91**, 2259–2272 (2004).
54. Boyden, E.S., Zhang, F., Bamberg, E., Nagel, G. & Deisseroth, K. Millisecond-timescale, genetically targeted optical control of neural activity. *Nat. Neurosci.* **8**, 1263–1268 (2005).